Available online at www.sciencedirect.com
SCIENCE DIRECT
Journal of Magnetic Resonance 180 (2006) 274–279
JMR Journal of Magnetic Resonance
www.elsevier.com/locate/jmr

Single-sided sensor for high-resolution NMR spectroscopy

J. Perlo, F. Casanova, B. Blümich *

Institut für Technische Chemie und Makromolekulare Chemie, RWTH Aachen, D-52056, Germany

Received 4 November 2005; revised 3 March 2006
Available online 31 March 2006

Abstract

The unavoidable spatial inhomogeneity of the static magnetic field generated by open sensors has precluded their use for high-resolution NMR spectroscopy. In fact, this application was deemed impossible because these field variations are usually orders of magnitude larger than those created by the microscopic structure of the molecules to be detected. Recently, chemical shift resolved NMR spectra were observed for the first time outside a portable single-sided magnet by implementing a method that exploits inhomogeneities in the rf field designed to reproduce variations of the static magnetic field [J. Perlo, V. Demas, F. Casanova, C.A. Meriles, J. Reimer, A. Pines, B. Blümich, High-resolution spectroscopy with a portable single-sided sensor, Science 308 (2005) 1279]. In this communication, we describe in detail the magnet system built from permanent magnets as well as the rf coil geometry used to compensate the static field variations.

Keywords: Single-sided NMR; Chemical shift; Mobile probes; Inhomogeneous magnetic fields

1. Introduction

Mobile single-sided probes have been used for NMR measurements over the last two decades [1–3]. They combine open magnet geometries and surface rf coils to measure NMR signals from arbitrarily sized samples in a noninvasive fashion. Sustained development of both hardware and methodology have led to portable systems with the capability to measure, for example, 3D images [4,5], velocity maps [6,7], and even multiple quantum coherences [8]. However, the strong inhomogeneity of the magnetic field precluded the use of NMR spectroscopy to determine molecular material composition, a fact that has limited single-sided NMR to the measurement of relaxation phenomena for sample characterization.

During the last years an ingenious technique developed by Meriles et al. has triggered a huge advance towards recovering high-resolution spectroscopy in single-sided sensors [9–15]. The methodology is based on the use of an inhomogeneous rf field with the spatial variation of the static magnetic field. In this case, the dephasing introduced during the application of an rf pulse is canceled by the phase accumulated during a subsequent free evolution period, leading to the formation of a so called nutation echo [9]. To prove the validity of this technique, experiments have been carried out inside superconducting magnets in the presence of a moderate static field gradient generated by the imaging gradient system (used to simulate the magnetic field inhomogeneity of open sensors). However, the state of the art of single-sided sensors in terms of both, magnetic field and gradient strength [3,4] delayed the implementation of the technique on real devices. It is worth noting that while the absolute difference in frequency between two chemical-shift lines is proportional to the field magnitude, the line-width is proportional to the gradient strength. Taking as a reference the original experiments conducted at high field (180 MHz), where a spectral resolution of 0.5 ppm was achieved in the presence of a uniform static gradient of 0.012 T/m (applied to spread the line over 10 ppm), the resolution achievable in a typical single-sided sensor can be estimated. For example, assuming that the same $B_0 - B_1$ matching quality can be achieved for the sensor described in [4], where $\nu_0 = 8$ MHz and $G_0 = 2.5$ T/m, a resolution of about 2300 ppm is predicted. Although this

* Corresponding author. Fax: +49 241 8022185.
E-mail addresses: fcasanova@mc.rwth-aachen.de (F. Casanova), bluemich@mc.rwth-aachen.de (B. Blümich).

1090-7807/$ - see front matter © 2006 Published by Elsevier Inc.
doi:10.1016/j.jmr.2006.03.004

factor already indicates how challenging the implementation of this methodology is on a low-field unilateral sensor, another serious complication needs to be considered: the field profile generated by a single-sided magnet can be quite complex because not only its magnitude but also its direction are likely to change along the three spatial dimensions, while in the idealized setup just a constant gradient along one defined spatial direction was used.

In spite of the initial predictions, we have recently measured the first NMR spectra outside the magnet with a portable sensor [16]. The key step in achieving the high matching quality required for this experiment was the use of an inverse shimming concept where the spatial dependence of $B_0(r)$ was shaped by varying the magnet geometry to copy the one of $B_1(r)$ generated by the surface rf coil. It must be noticed that the original approach where the coil geometry is optimized to match the static field generated by an arbitrary magnet could easily lead to a sensitivity loss of several orders of magnitude.

In this paper, we present an extended description of the magnet and rf coil designs that allowed us to measure chemical shift spectra from different fluorinated liquids with a spectral resolution of about 8 ppm in experimental times of the order of 3 min [16].

2. Magnet and rf coil optimization

The open magnet built for this work is composed of two units, a main magnet (M) and a shimming unit (S), both built from NbFeB permanent magnets with a remanent flux density of 1.33 T, a coercive field strength of 796 kA/m, and a temperature coefficient of 400 ppm/°C. The main unit has a classical U-shaped geometry, which consists of two magnet blocks with opposite polarization placed on an iron yoke leaving a gap between them (Fig. 1) [17]. It has been used before for imaging applications, where the rf coil was placed at 3 cm from the magnet surface to exploit the uniform gradient defined there for slice selection. For this work, however we found it more convenient to work closer to the surface of the magnet, where the set-up generates a magnetic field of about 0.250 T along z with a main gradient of about 0.4 T/m along the depth direction y. The magnetic field varies also along the lateral directions, so that in a small volume close to the y-axis the field profile in both directions can be well approximated by quadratic functions.

In a first attempt to implement this methodology, a number of rf coil geometries were shaped to copy the spatial dependence of B_0 generated by the main unit, but the optimization procedure systematically led to large coils of extremely poor sensitivity. The problem can easily be explained when observing the spatial dependence of the static field generated by this magnet and the rf field generated by, for example, a rectangular coil (Fig. 2). Although the fields can be matched in a reasonably large region along the depth direction (Fig. 2A), the rf field reproduces the lateral variation of the static field only at one defined distance

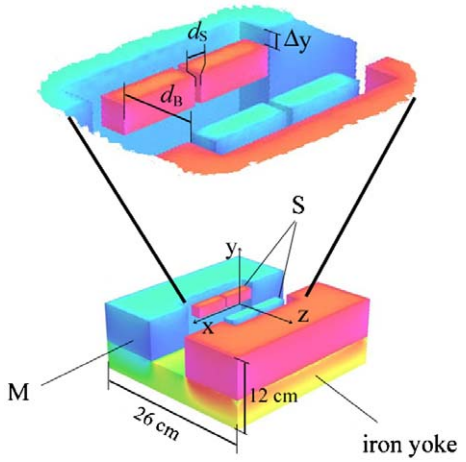

Fig. 1. Magnet system. The main unit (M) is a classical U-shaped magnet, where two magnets blocks with opposite polarization are placed on an iron yoke leaving a gap between them (10 cm in the central region up to $x = 13$ cm, and 8 cm at the borders). The shimming unit (S) produces a field with opposite sign and a gradient comparable to the main one. The color scale represents the y component of B_0 to show the polarization sign of the different magnet blocks. The total magnet assembly generates a static field of about 0.2 T in the region of interest and weights about 36 kg.

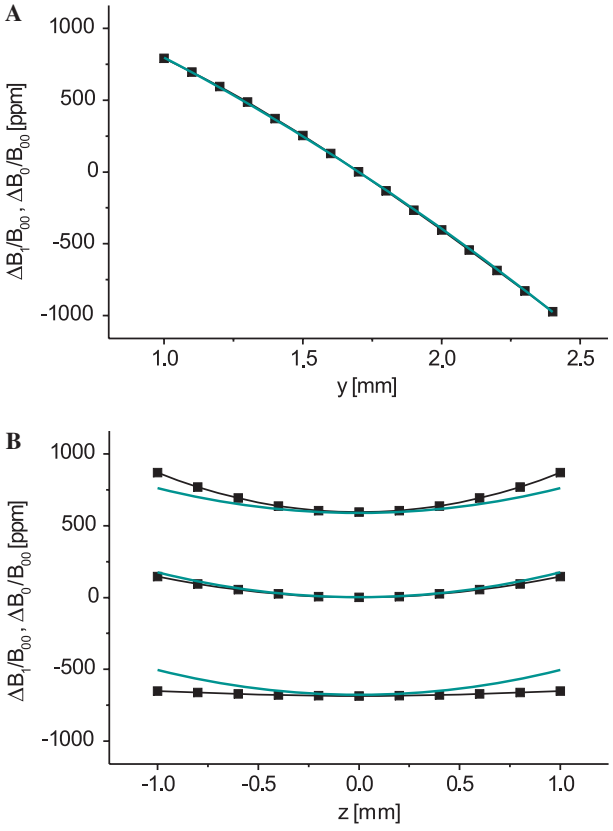

Fig. 2. Static (–) and rf (■) fields generated by the main unit and a rectangular rf coil, respectively. (A) Spatial dependence along the depth direction. Both fields posses a quadratic dependence that can be matched in a reasonably large region. The origin of the coordinate system is chosen at the surface of the magnet, and the rf coil is located at 1 mm from the surface. (B) Along the lateral direction z both fields vary in a parabolic fashion, but their quadratic coefficients depend differently on depth. While for the magnet the coefficient remains almost constant, for the rf field it even changes sign so that at a certain depth, the lateral variation vanishes.

from the coil surface (Fig. 2B). Although both fields posses parabolic profiles, their quadratic coefficients vary in a different way as a function of the depth. While for the static field, the field profile remains almost constant, it varies for the rf field. To reduce this variation to improve the matching in the region plotted in Fig. 2, the coil dimensions must be increased. But by doing so, the sensitivity of the rf coil decreases. This is why an inverse approach was taken, where the magnet geometry was varied to improve the $B_0 - B_1$ matching over a sufficiently large volume while keeping the coil dimensions fixed.

A rectangular rf coil like the one shown in Fig. 3 generates an rf field whose component perpendicular to B_0 has a spatial dependence that can be expanded as

$$B_{\perp 1}(\vec{r}) = B_{10} + g_{1y}y' + (\alpha_{1z}y')z^2 + (\alpha_{1x}y')x^2. \quad (1)$$

It has a main gradient g_{1y} along the depth direction, and lateral variations that can be well approximated by parabolas with quadratic coefficients varying linearly with the depth. The value of α_{1x}, and α_{1z} can be controlled independently by varying the coil dimensions L_x and L_z, respectively. When the coil sides are different, the lateral variations along x and z vanish at different depths. Nevertheless, these positions can be matched in a particular depth ($y' = 0$ in Eq. (1)) by winding the wires parallel to x and z in planes separated by a distance δ_y (Fig. 3).

The new matching strategy required the incorporation of variables in the magnet geometry to shape the spatial dependence of the magnetic field, and, at the same time, to reduce the static field gradient strength. Both goals were achieved by adding a shim magnet in the gap of the main magnet. It consists of four permanent magnet blocks $45 \times 15 \times 15\ \text{mm}^3$ arranged in a U-shaped configuration but without iron yoke. The blocks with same polarization are separated by a small gap d_S, while between pairs with opposite polarization there is a gap d_B. Although the shim magnet generates a magnetic field weaker than the one produced by the main unit, the gradients along x, y, and z of both fields are comparable. Therefore by choosing opposite polarizations between the two units and placing the shim unit as shown in Fig. 1, the gradients can be made to approximately cancel each other. As mentioned before, the lateral variations of the field produced by the main unit can be approximated by parabolas with coefficients that do not depend on the depth. This is also the case for the S unit. However, with its dimension being smaller than that of the M unit, the quadratic coefficients change slightly with the depth. As a consequence, when both units are combined, the total field has quadratic coefficients that vary linearly with depth from negative to positive values (Eq. (2)). This fact is extremely useful to reproduce the field profile of the rf coil.

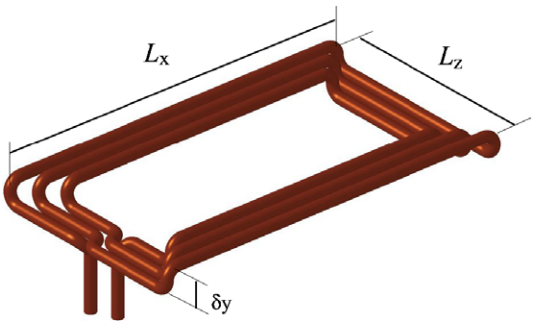

Fig. 3. Rectangular surface rf coil wound from 0.45 mm diameter copper wire. By varying the vertical distance δ_y between the wires along x and z and the lengths L_z and L_x, the spatial dependence of the rf field can be controlled.

To a good extent, the direction of the magnetic field produced by the full magnet can be considered to point along z, and its magnitude can be approximated by

$$B_0(\vec{r}) = B_{00} + g_{0y}y + (\alpha_{0z}y)z^2 + (\alpha_{0x}y)x^2. \quad (2)$$

Along y the field has a constant gradient g_{0y} whose magnitude and even sign can be modified by varying the relative distance Δy, and along both lateral directions the field has quadratic dependences with coefficients that depend on the size of the shimming unit. In Eq. (2) it is assumed that both lateral variations vanish at the same depth from the surface of the main magnet, and this particular position is defined as the new $y = 0$. Actually, this condition is not always reached at the same depth for x and z, but it can be achieved by adjusting independently the gaps d_B and d_S.

3. Matching

The condition required for the formation of nutation echoes requires the combination of B_0 and B_1 fields with spatial dependences scaled by a free factor κ. It can be written as

$$\frac{dB_{1\perp}(\vec{r})}{dr} = \kappa \frac{dB_0(\vec{r})}{dr}, \quad (3)$$

where κ is a scalar that does not depend on space coordinates. By integrating with respect to space variables Eq. (3) becomes

$$B_{1\perp}(\vec{r}) = \kappa B_0(\vec{r}) + \omega_{10}/\gamma, \quad (4)$$

where the constant ω_{10}/γ is associated to the undefined zero of the chemical shift frequency discussed in [9]. This equation is more convenient than Eq. (3) because it is expressed in terms of magnetic fields and not in terms of derivatives. By replacing B_1 and B_0 by the expansions of Eqs. (1) and (2), and assuming that the relative position between the magnet and rf coil is adjusted to $y = y'$, the following conditions are obtained

$$\frac{g_{1y}}{g_{0y}} = \frac{\alpha_{1z}}{\alpha_{0z}} = \frac{\alpha_{1x}}{\alpha_{0x}} = \kappa. \quad (5)$$

As mentioned above, both the magnet and the rf coil were built in a way that the spatial variations along x, y, and z (associated with α_{ix}, α_{iz}, and g_{iy}, $i = 0, 1$) are almost decou-

pled. Furthermore, it is possible to adjust the value of each coefficient by controlling d_B, d_S, and Δy for the magnet, and L_x, L_z, and δ_y for rf coil.

The steps followed during the matching procedure can be summarized as follows. First, the dimensions of the rectangular coil were defined and the coefficients describing the rf field were calculated. Second, the geometry of the shim unit was optimized so that, in combination with the main unit, a total magnetic field was generated with the same spatial dependence as the one of the rf field. This optimization was done numerically by calculating the total magnetic field as the sum of the magnetic fields generated by the main unit (measured with a Hall sensor) and the field generated by the shim unit (calculated numerically). Once the dimensions and positions of the magnets of the shim unit were determined, they were mounted in an aluminium holder, which was later placed in the gap of the main magnet. The units were assembled by displacing the shim unit in a vertical trajectory from large depths inside the gap. When the shim unit surface is above the main unit, both units repel each other, so that a force is required to join them. But once its center crosses the surface of the main magnet, the gradient of the static field changes sign, and both units strongly attract each other. At the final position, the attracting force is estimated to be about 250 N. This fact is of considerable advantage because the attraction provides stability to the entire magnet, avoiding the need of an extra holder required in case of repulsion.

After combining the magnet units, the total field was scanned with a precision better than 5 μT via the resonance frequency of a tiny oil sample with a thickness of 0.1 mm and a surface area of $1 \times 1\ \text{mm}^2$. With the help of this high-resolution measurement, the shim unit was positioned in the gap of the main unit, and the fine tuning of d_S and d_B was achieved to match the depth positions, where the lateral variations along x and z vanish. For this purpose, the shim unit was equipped with a set of bolts along the three axes that provided a positioning precision of about 20 μm. Notice, that by scanning the total field of the magnet, possible defects in the magnet manufacturing processes, which are typical for this type of material, can also be detected.

Finally, the rf coil was built taking into account the final coefficients of the static field, which were calculated from the scanned data. Actually, the new dimensions did not differ appreciably from the original ones assumed for the magnet calculation. The coil was mounted on a movable plate that allowed its positioning with a precision of about 20 μm. The final parameters obtained after optimization are $d_B = 42$ mm, $d_S = 5.8$ mm, and $\Delta y = 8$ mm for the magnet, and $L_x = 14$ mm, $L_z = 9$ mm, and $\delta_y = 1$ mm for the rf coil. To match the plane where the lateral variation of both B_0 and B_1 vanish ($y = y'$), the rf coil was placed 4.5 mm above the main magnet surface. The position $y = 0$ is 2 mm above the rf coil, and there the magnetic field reaches 0.2 T. For this configuration, the coefficients of the field are $g_{0y} = 205$ ppm/mm (0.04 T/m), $\alpha_{0z} = 47$ ppm/mm^3, and $\alpha_{0x} = 4.4$ ppm/mm^3. For comparison, the main magnet generates a field of 0.24 T at this position with a main gradient of 3700 ppm/mm (0.9 T/m).

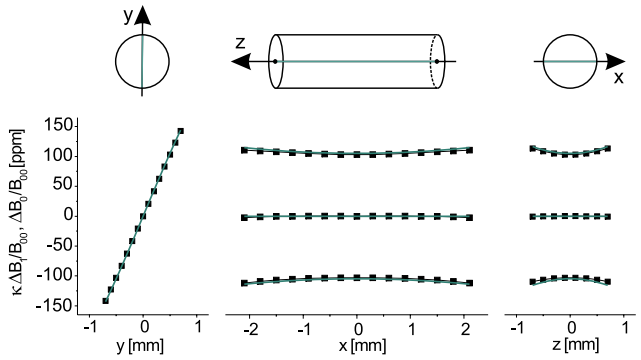

Fig. 4. Spatial variation of the static (–) and rf (■) fields. Both B_0 and B_1 follow the spatial dependence described in Eqs. (1) and (2). While a linear dependence is observed along the depth direction, both lateral variations along x and z show a parabolic dependence with quadratic coefficients that change sign as a function of the depth (the lateral variations are plotted at depths of 0.5, 0, and −0.5 mm). For better visualization, both fields were divided by B_{00}, and the variations in ppm was referred to the value at the coordinate origin. The parameters found for obtaining this field variation are $d_B = 42$ mm, $d_S = 5.8$ mm, and $\Delta y = 8$ mm for the magnet, and $L_x = 14$ mm, $L_z = 9$ mm, and $\delta_y = 1$ mm for the rf coil. For these parameters one obtains $g_{0y} = 205$ ppm/mm (0.04 T/m), $\alpha_{0z} = 47$ ppm/mm^3, and $\alpha_{0x} = 4.4$ ppm/mm^3. The rf coil was placed 4.5 mm above the main magnet surface to fulfill the condition $y = y'$. The position where both lateral variations vanish ($y = 0$) is 2 mm above the rf coil and there the magnetic field reaches 0.2 T.

To visualize the matching quality obtained with the final configuration, the variations of B_0 and B_1 fields were normalize to B_{00} and expressed in ppm, where B_{00} is the field value at the origin of the coordinate system (Fig. 4). For simplicity the proportional factor was set to be $\kappa = -1$. The difference between the B_0 and B_1 curves in Fig. 4 gives direct evidence of the field matching across the volume of the sample. It is interesting to notice that the coefficients describing the lateral variations of both the magnetic and the rf fields are of opposite sign. Since the rf field decays with the distance from the coil, the static field must increase with the depth to achieve $\kappa = -1$. This is obtained by using a shim unit which produces a main gradient stronger than the one produced by the main magnet. It is important to stress that the final magnet configuration does not minimize the gradient along the depth direction, but retains the value required to match the gradient of the rf field. It must be understood, that the shim unit is not used to shim the static field to homogeneity but to reproduce the inhomogeneity of the rf field.

4. Results

The aim of this section is to show in steps how the spectral resolution was improved to a final value of 8 ppm; which is good enough to clearly discriminate chemical shifts of different fluorinated fluids [16]. For the experi-

ment, a capillary tube with an inner diameter of 1 mm and a length of 3 mm was placed on the magnet with its axis along x. The positioning of the sample requires a precision of the order of a fraction of the total volume where the desired matching is achieved. In the present case this volume is approximately 1 mm along every direction, and once the optimum position was found, we did not observe appreciable resolution loss even when misplacing the sample by 200 μm. Fig. 5A shows the Fourier transform of the echo signal measured in the field generated by the main magnet. A broad line covering a range of about 3000 ppm is obtained. By including the shimming unit in the gap of the main magnet the frequency spread is reduced to 200 ppm (Fig. 5B). Finally, by implementing the nutation echo experiment [16] a spectral resolution of 8 ppm could be obtained (Fig. 5C). The three ^{19}F chemical shift signals of a mixture of hexafluorobenzene and perfluorohexane are clearly resolved. The positions and relative amplitudes of the different lines are in agreement with the results measured by conventional high-field magnets. More detailed information about the pulse sequence can be found in [16].

The spectral resolution offered by this method is determined by the matching quality achieved in the sample volume. This situation can directly be compared to the use of shim fields in conventional NMR with homogeneous fields, where the resolution is limited by how well the currents in the shim coils are set to compensate the variations of the main field across the sample. As in conventional homogeneous field experiments, the maximum resolution attainable with the present method is also limited, in the ultimate case of perfect matching, by the T_2 of the sample.

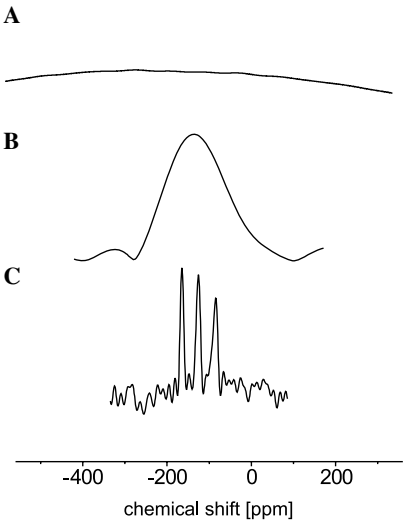

Fig. 5. (A) NMR spectrum measured with a U-shaped magnet (M unit in Fig. 1). (B) Spectrum measured including the shim unit (S unit in Fig. 1). (C) Spectrum measured with the nutation echo experiment. The three ^{19}F chemical shift signals correspond to the C_6F_6, CF_3, and CF_2 groups in the mixture hexafluorobenzene and perfluorohexane. The total experimental time was only 3 min.

5. Conclusions

The construction of the first mobile open sensor for high-resolution NMR spectroscopy has been described. The use of small permanent magnet blocks to shim the static magnetic field has been extremely useful not only to model the spatial B_0 variations to match the B_1 field, but also to reduce the static gradient strength. The inverse shimming concept, where the magnet is built to match the B_1 inhomogeneities, led to a spectral resolution of 8 ppm.

Taking into account that only 3 min were needed to measure spectra with such a resolution, ^1H chemical shift resolved spectra could be attainable simply by reducing the sample size and at the expense of a longer measuring time. However, this solution must be carefully analyzed: the longer the measuring time and the better the spectral resolution, the more sensitive becomes the experiment to frequency drifts arising from changes in the magnet temperature. Although in this work no temperature control was required, temperature stabilization units will become necessary in the future.

New calculations, based on a different shim unit geometry, have shown that a resolution of about 1 ppm can be obtained in the same volume. This value could be further improved either by the use of single-sided shim coils, by implementing the "shim pulses" recently reported by the Pines group [15], or by a combination of both. Based on these facts, we can anticipate that in the near future ^1H chemical-shift resolved spectra can realistically be measured with unilateral low-field devices. Like for conventional superconducting magnets, the volume where high-resolution spectra can be measured is limited. In the present work this volume is about 3 mm^3. To extend the application of this technique to arbitrarily sized samples, which is the general case for single-sided NMR, a volume selection technique is required.

Acknowledgments

This project was supported by DFG Forschergruppe FOR333 "Surface NMR of Elastomers and Biological Tissues." We are grateful to V. Demas, C.A. Meriles, J. Reimer, and A. Pines for helpful discussions during the course of this work. Many thanks go to K. Kupferschläger, S. Harms, M. Küppers, J. Kolz, and C. Terlinden.

References

[1] J.A. Jackson, L.J. Burnett, F. Harmon, Remote (Inside-Out) NMR. III. Detection of nuclear magnetic resonance in a remotely produced region of homogeneous magnetic field, J. Magn. Reson. 41 (1980) 411–421.

[2] R.L. Kleinberg, A. Sezginer, D.D. Griffin, M. Fukuhara, Novel NMR apparatus for investigating an external sample, J. Magn. Reson. 97 (1992) 466–485.

[3] G. Eidmann, R. Salvelsberg, P. Blümler, B. Blümich, The NMR-MOUSE, a mobile universal surface explorer, J. Magn. Reson. A 122 (1996) 104–109.
[4] J. Perlo, F. Casanova, B. Blümich, 3D imaging with a single-sided sensor: an open tomograph, J. Magn. Reson. 166 (2004) 228–235.
[5] J. Perlo, F. Casanova, B. Blümich, Profiles with microscopic resolution by single-sided NMR, J. Magn. Reson. 176 (2005) 64–70.
[6] F. Casanova, J. Perlo, B. Blümich, Velocity distributions remotely measured with a single-sided sensor, J. Magn. Reson. 171 (2004) 124–130.
[7] J. Perlo, F. Casanova, B. Blümich, Velocity imaging by ex-situ NMR, J. Magn. Reson. 173 (2005) 254–258.
[8] A. Wiesmath, C. Filip, D.E. Demco, B. Blümich, NMR of multipolar spin states excitated in strongly inhomogeneous magnetic fields, J. Magn. Reson. 144 (2002) 60–72.
[9] C.A. Meriles, D. Sakellariou, H. Heise, A.J. Moulé, A. Pines, Approach to high-resolution ex situ NMR spectroscopy, Science 293 (2001) 82–85.
[10] D. Sakellariou, C. Meriles, A. Moulé, A. Pines, Variable rotation composite pulses for high resolution NMR using inhomogeneous magnetic and radiofrequency fields, Chem. Phys. Lett. 363 (2002) 25–33.
[11] C.A. Meriles, D. Sakellariou, A. Pines, Resolved magic-angle spinning of anisotropic samples in inhomogeneous fields, Chem. Phys. Lett. 358 (2002) 391–395.
[12] C.A. Meriles, D. Sakellariou, A. Pines, Broadband phase modulation by adiabatic pulses, J. Magn. Reson. 154 (2003) 177–181.
[13] C.A. Meriles, D. Sakellariou, A. Moulé, M. Goldman, T. Budinger, A. Pines, High-resolution NMR of static samples by rotation of the magnetic field, J. Magn. Reson. 169 (2004) 13–18.
[14] V. Demas, D. Sakellariou, C.A. Meriles, S. Han, J. Reimer, A. Pines, Three-dimensional phase-encoded chemical shift MRI in the presence of inhomogeneous fields, Proc. Natl. Acad. Sci. USA 101 (2004) 8845–8847.
[15] D. Topgaard, R. Martin, D. Sakellariou, C.A. Meriles, A. Pines, Shim pulses for NMR spectroscopy and imaging, Proc. Natl. Acad. Sci. USA 101 (2004) 17576–17581.
[16] J. Perlo, V. Demas, F. Casanova, C.A. Meriles, J. Reimer, A. Pines, B. Blümich, High-resolution spectroscopy with a portable single-sided sensor, Science 308 (2005) 1279.
[17] H. Popella, G. Henneberger, Design and optimization of the magnetic circuit of a mobile nuclear magnetic resonance device for magnetic resonance imaging, COMPEL 20 (2001) 269–278.